Progress In Electromagnetics Research, Vol. 127, 259–275, 2012

APPLICATIONS OF COMPRESSED SENSING FOR MULTIPLE TRANSMITTERS MULTIPLE AZIMUTH BEAMS SAR IMAGING

J. Li*, S. S. Zhang, and J. F. Chang

Research Institute of Electronic Science and Technology, University of Electronic Science and Technology of China, Chengdu 611731, China

Abstract—High speed analog-to-digital (A/D) sampling and a large amount of echo storage are two basic challenges of high resolution synthetic aperture radar (SAR) imaging. In this paper, a novel SAR imaging algorithm which named CS-MTMAB is proposed based on compressed sensing (CS) and multiple transmitters multiple azimuth beams (MTMAB). In particular, this new algorithm, which respectively reconstructs the targets in range and azimuth directions via CS technique, simultaneously provides a high resolution and wide-swath two-dimensional map of the spatial distribution of targets with a significant reduction in the number of data samples beyond the Nyquist theorem and with an implication in simplification of radar architecture. The simulation results and analysis show that this new imaging scheme allows the aperture to be compressed and presents many important applications and advantages among which include reduced on-board storage constraints, higher resolution, lower peak side-lobe ratio (PSLR) and integrated side-lobe ratio (ISLR), less sampled data than the traditional SAR imaging algorithm, and also indicate that it has high robustness and strong immunity in the presence of serious noise. Finally, the real raw airborne SAR data experiment is performed to validate the proposed processing procedure.

1. INTRODUCTION

Synthetic aperture radar (SAR) is a radar imaging technology that is capable of producing high resolution images of the stationary surface targets [1]. The main advantages of SAR are that it can reduce the effects of clouds and fog and allow them to be independent of

Received 13 February 2012, Accepted 18 March 2012, Scheduled 16 April 2012

* Corresponding author: Jing Li (lijing8609@hotmail.com).

external sources for imaging, having day and night and all-weather imaging capability. Traditional compressions of SAR data utilize the redundancy inherent in sampled data under the Nyquist theorem to achieve compressed representation and profitable transmission. This theory claims that one must sample at least two times faster than the signal bandwidth while capturing it without losing information. Thereby there are large amounts of onboard data that have to be stored and it inevitably results in complex computation and expensive hardware.

On the other hand, future SAR will be required to produce high-resolution image over a wide area of surveillance. However, minimum antenna area constraint makes it a contradiction to obtain both high azimuth resolution and wide-swath simultaneously, which is derived form the inconsistent requirements for pulse repetition frequency (PRF). According to the Nyquist Theorem, to reconstruct an unambiguous azimuth profile, the sampling rate of the azimuth must not be less than its Doppler bandwidth. A high azimuth sampling rate could be a restriction on the swath. To address the problems, the multiple transmitters multiple azimuth beams (MTMAB) SAR has been proposed in [2–7]. By using MTMAB SAR system, additional samples are received for each transmitted pulse. This allows for a reduced pulse repletion frequency thereby enabling a wide swath.

The recently introduced theory of compressed sensing (CS) states that it is possible to recover sparse images from a small number of random measurements, provided that the undersampling results in noise like artifacts in the transform domain and an appropriate nonlinear recovery scheme is used [8–11]. CS is a new concept allowing recovery of signals that have been sampled below the traditional Nyquist sampling rate. In this new framework, it uses a low-dimensional, nonadaptive, linear projection to acquire an efficient representation of a sparse signal with just a few measurements, so as to greatly reduce the sampling rate and enhance the data rate. Because of its compressed sampling ability, compressed sensing has found many applications in radar and remote sensing, and other fields. Baraniuk and Steegh [12] propose lowering the rate of the A/D converter in the receive based on the notion of CS. In [13], a high resolution radar was proposed based on CS by transmitting specially designed waveforms. In [14], sparse signal representation and approximations from complete dictionaries are explored. Patel et al. [15] use CS to focus inverse SAR images of airplanes that have already been motion compensated. Wei et al. [16, 17] analyzed high resolution properties of CS in SAR 2-D imaging and linear array SAR imaging, but the results demonstrate that CS method is sensitive to noise, and the exact reconstruction

requires high SNR level of raw echo. And some major open questions related with the application of CS to SAR and ISAR are listed in [18].

In this paper, we introduce a novel synthetic aperture radar imaging algorithm which named CS-MTMAB based on compressed sensing (CS) theory and multiple transmitters multiple azimuth beams (MTMAB) techniques. Our approach is in contrast to other compressive radar related algorithms that have only considered using CS as part of one-dimensional analog-to-information conversion. The key idea in our approach is to use CS to reconstruct two-dimensional (2-D) target in the range dimension and azimuth dimension, respectively. This radar system randomly transmits fewer pulses in azimuth direction and samples fewer data than traditional systems at random intervals in range direction. In addition, the proposed algorithm can reduce the required receiver analog-to-digital (A/D) conversion bandwidth so that it need operate only at the reflectivity's potentially low "information rate" rather than at its potentially high Nyquist rate [12]. We present two extraordinary and innovative applications of CS for MTMAB SAR. 1) The algorithm achieves 2-D imaging of the targets via constructing the range measurement matrix and the azimuth measurement matrix using CS. 2) The MTMAB technology is used in this algorithm to resolve the contradiction between high resolution and wide-swath. This will directly impact A/D conversion, and has the potential to reduce the overall data rate and to simplify hardware design. Meanwhile, it provides the potential to achieve higher resolution between targets. More importantly, our method does not use a matched filter and enhances some of these suggestions and provides a proper framework along with general reconstruction techniques.

The rest of this paper is organized as follows. In Section 2, the basic theory of compressed sensing is presented. In Section 3, the signal model and the image formation algorithm using CS are discussed in detail. The results of performance analysis and the real data experimental results are presented in Section 4. Finally, Section 5 concludes this paper.

2. COMPRESSED SENSING

The Shannon-Nyquist sampling theorem requires a signal to be sampled at a frequency of twice its bandwidth to be able to reconstruct it exactly. In CS framework, it uses a low-dimensional, nonadaptive, linear projection to acquire an efficient representation of a sparse signal with just a few measurements, so as to greatly reduce the sampling rate and enhance the data rate. According to the compressed sensing theory [8–10], there are three important ingredients: sparse signal

representation, measurement operator, and sparse reconstruction algorithms. Consider a discrete signal expressed as a vector $\mathbf{x} \in \mathbb{C}^N$ of length N. Suppose $\mathbf{x}$ is *K-sparse* if at most $K \ll N$ of its coefficients are nonzero in a basis or more generally a frame $\mathbf{\Psi}$, so that $\mathbf{x} = \mathbf{\Psi s}$, where $\mathbf{\Psi} \in \mathbb{C}^{N \times N}$ is a sparsity basis matrix and $\mathbf{s} \in \mathbb{C}^N$ is a vector. The signal is acquired through linear projections:

$$\mathbf{y} = \mathbf{\Phi x} = \mathbf{\Phi \Psi s} = \mathbf{\Theta s} \tag{1}$$

where $\mathbf{y} \in \mathbb{C}^M$ is the measurement vector and $\mathbf{\Phi} \in \mathbb{C}^{M \times N}$ is the measurement matrix with $M < N$. Since $M < N$, the recovery of signal $\mathbf{x}$ from the measurement vector $\mathbf{y}$ is ill-posed in general. But when the matrix $\mathbf{\Theta}$ has the Restricted Isometry Property (RIP) [19], it is possible to reconstruct $\mathbf{x}$ from a set of $M = O(K \log(N/K))$ linear measurements. The RIP requires that

$$(1 - \delta_K) \|\mathbf{s}\|_2^2 \leq \|\mathbf{\Theta s}\|_2^2 \leq (1 + \delta_K) \|\mathbf{s}\|_2^2 \tag{2}$$

where $\mathbf{s}$ is any vector having K nonzero coefficients, and $\delta_K \in (0, 1)$. The signal $\mathbf{x}$ can be perfectly recovered via its coefficients $\mathbf{s}$ with high probability, by solving the following l_0 minimization problem:

$$\hat{\mathbf{s}} = \arg\min \|\mathbf{s}\|_{\mathbf{0}} \quad s \cdot t \cdot \mathbf{y} = \mathbf{\Phi \Psi s} = \mathbf{\Theta s} \tag{3}$$

Unfortunately, solving (3) is an NP problem and minimum l_0 norm is too sensitive to noise. Consequently, the researchers [19] present that the recovery of sparse coefficients $\mathbf{s}$ can be achieved using optimization by searching for the signal with a l_1 minimization problem:

$$\hat{\mathbf{s}} = \arg\min \|\mathbf{s}\|_{\mathbf{1}} \quad s \cdot t \cdot y = \mathbf{\Phi \Psi s} = \mathbf{\Theta s} \tag{4}$$

The optimization problem (4) is often known as Basis Pursuit (BP) and Orthogonal Matching Pursuit (OMP) which can be solved by linear programming methods.

3. CS APPLIED FOR MTMAB SAR

3.1. Signal Model

Figure 1 (an example of three antennas) shows the geometry of MTMAB SAR and how received data are placed in a three-dimensional (3-D) signal model. Compared to a single-aperture system, each antenna of MTMAB SAR system receives and transmits signals. Multiple receivers gather for the same PRF in azimuth dimension, thereby ensuring constant performance over a clearly extended PRF range. As the radar moves along its path in azimuth direction, it transmits pulses at microwave frequencies at a random pulse repetition interval (PRI) which is defined as 1/PRF. Instead of sampling in range

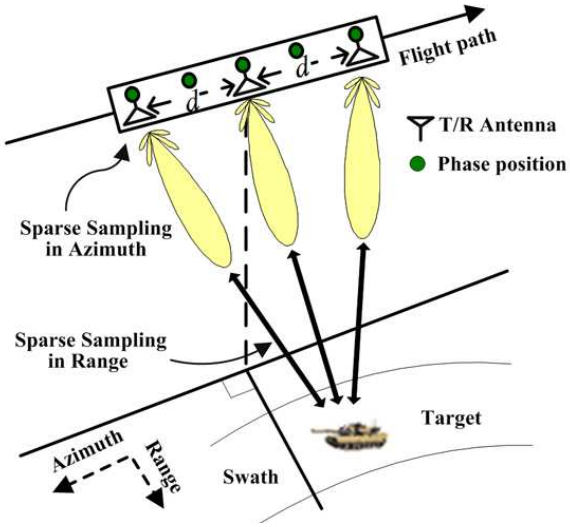

Figure 1. Geometry of 2-D random sparse sampling for MTMAB SAR.

direction with a regular interval, we propose to sample fewer data than traditional systems at random intervals.

Suppose K is the antenna number, according to the theory of MTMAB SAR, there are $2K-1$ equivalent phase centre positions [20]. The antenna positions are governed by the spacing d of the K receivers in combination with the distance between subsequent pulses given by the sensor velocity v and PRF. Consequently, a uniform sample distribution is obtained only if the following timing requirement is fulfilled [20]:

$$d = \frac{2v}{(2K-1) \times \mathrm{PRF}} \tag{5}$$

Thus, the virtual uniform linear array is composed of the equivalent phase centre positions, as shown in Figure 2. By this, the equivalent phase centre positions of the MTMAB SAR system are adjusted from pulse to pulse in order to match them to the PRF, thus increasing the usable PRF range.

3.2. Imaging Formation Algorithm Using CS

As shown in Figure 1, a scatter within that scene is located at $\mathbf{P} = (x, y, 0)$. $R_T(\eta; \mathbf{P})$ and $R_R(\eta; \mathbf{P})$ denote the slant ranges from scatterer $\mathbf{P}$ to the transmitter and the receiver, respectively, where η

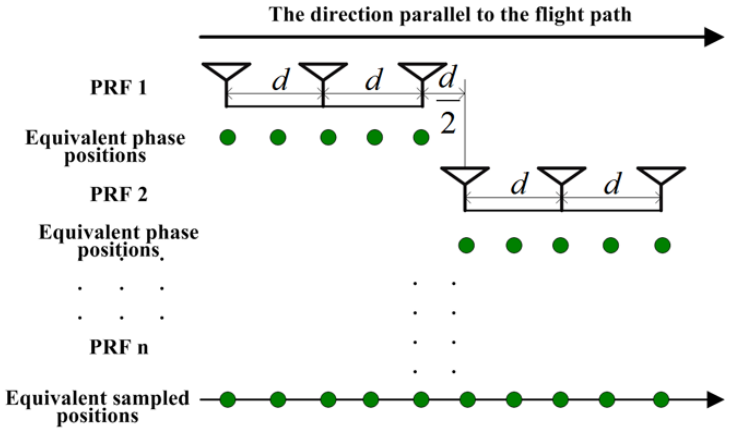

Figure 2. MTMAB SAR system with uniform displaced phase center sampling.

represents the slow time. Suppose the k-th antenna transmits signals and the l-th antenna receives echo signals. The sum of the range from the k-th transmitter and the l-th receiver to the target $\mathbf{P}$ can be written as

$$\begin{aligned} R_{kl}(\eta;\mathbf{P}) &= R_T(\eta;\mathbf{P}) + R_R(\eta;\mathbf{P}) \\ &= \sqrt{R_{T0}^2 + (v\eta - kd - x)^2} + \sqrt{R_{R0}^2 + (v\eta - ld - x)^2} \end{aligned} \quad (6)$$

where R_{T0} and R_{R0} are the transmitted and received range to the sensor position at $\eta = 0$, respectively, and v represents the sensor velocity, d represents the space of received antennas, x is the azimuth coordinate of target $\mathbf{P}$. Suppose the transmitted signal is linear frequency modulated (LFM) signal which can be described as

$$s_T(\tau) = \text{rect}\left(\frac{\tau}{T_p}\right) \exp\left\{j2\pi f_c\tau + j\pi k_r\tau^2\right\} \quad (7)$$

where T_p is the pulse duration, τ is the fast time, f_c is the carrier frequency, k_r is the chirp rate and rect $(\cdot)$ is the stand for the unit rectangular function. After mixing down and quadrature demodulation, the received radar signal is given by

$$\begin{aligned} s_R(\tau,\eta) &= \text{rect}\left(\frac{\tau - R_{kl}(\eta;\mathbf{P})/c}{T_p}\right) \\ &\quad \times \exp\left\{j\pi k_r\left(\tau - \frac{R_{kl}(\eta;\mathbf{P})}{c}\right)^2 - j\frac{2\pi R_{kl}(\eta;\mathbf{P})}{\lambda}\right\} \end{aligned} \quad (8)$$

where c is the speed of light, and λ is the wavelength of the transmitted signal.

On the other hand, from the signals and systems of view, suppose $s_T(\tau)$ is the transmitted signal and the target is described by $u(\tau)$, then the received signal $s_R(\tau)$ can be written as [12]

$$s_R(\tau) = G \int s_T(\tau - \xi) u(\xi) d\xi \tag{9}$$

where G represents attenuation due to propagation and reflection. Consider a target reflectivity generated from N Nyquist-rate samples $x(n)$ via $x(n) = u(\Delta t)$, $n = 1, \ldots, N$. We sample the received radar signal $s_R(\tau)$ not every Δt seconds but rather random $\omega(m)\Delta t$ seconds, where $M = [N/D]$ and $M < N$, $\omega(m)$ is a random sequence of size $1 \times M$, to obtain the M samples, $m = 1, \ldots, M$

$$\begin{aligned} y(m) =& \left. s_R(\tau)\right|_{\tau=\omega(m)\cdot\Delta t} = G\int_0^{N\Delta t} s_T\left(\omega(m)\cdot\Delta t - \xi\right) u(\xi)\, d\xi \\ =& G\sum_{n=1}^{N} s_T(\omega(m)\cdot\Delta t - n)\int_{(n-1)\Delta t}^{n\Delta t} u(\xi) d\xi = G\sum_{n=1}^{N} s_T(\omega(m) - n) x(n) \end{aligned} \tag{10}$$

where $s_T(n)$ is the discrete transmitted signal. The low-rate samples y contain sufficient information to reconstruct the signal x corresponding to the Nyquist-rate samples of the reflectivity $u(\tau)$ via linear programming or a greedy algorithm.

It is well known that (10) is equal to a CS problem. In terms of (10), suppose D_r represents the down-sampling times in range direction, the range measurement matrix can be expressed as

$$\mathbf{\Phi_r}(m,n) = s_T(\omega(m) - n) = \mathrm{rect}\left(\frac{\omega(m) - n}{T_p}\right) \exp\left\{ j\pi k_r (\omega(m) - n)^2 \right\} \tag{11}$$

where $\mathbf{\Phi_r} \in \mathbb{C}^{M\times N}$, $M = N/D_r$, $m = 1, \ldots M$, $n = 1, \ldots N$. After the targets being reconstructed in range dimension via CS, the signal can be approximated as

$$s_{cs}(\tau, \eta) \approx \sin c\left(\tau - \frac{R_{kl}(\eta; \mathbf{P})}{c}\right) \exp\left\{ -j\frac{2\pi R_{kl}(\eta; \mathbf{P})}{\lambda} \right\} \tag{12}$$

where $\sin c(\cdot)$ is the Sinc function. The second factor of (12) is the Doppler phase factor. Similarly, suppose D_a represents the down-sampling times in azimuth direction, the azimuth measurement matrix

can be given by

$$\begin{aligned}\mathbf{\Phi_a}(q,p) &= \exp\left\{-j2\pi\frac{R_{kl}\left(q,p;\mathbf{P}\right)}{\lambda}\right\}\\ &= \exp\left\{-j2\pi\frac{\sqrt{R_{T0}^2+\left[v(w(q)-p)-kd-x\right]^2}}{\lambda}\right.\\ &\quad\left.-j2\pi\frac{\sqrt{R_{R0}^2+\left[v(w(q)-p)-ld-x\right]^2}}{\lambda}\right\}\end{aligned}\tag{13}$$

where $\mathbf{\Phi_a} \in \mathbb{C}^{Q\times P}$, $p = 1, \ldots P$ is the Nyquist sampling sequence in azimuth, $Q = P/D_a$, $q = 1, \ldots Q$ is the down-sampling sequence, $\omega(q)$ is the random sequence of size $1 \times Q$. After constructing $\mathbf{\Phi_r}$ and $\mathbf{\Phi_a}$, the Equation (4) can solve by OMP or BP in range and azimuth dimension, respectively. The procedure of MTMAB imaging algorithm using CS is shown in Figure 3. Obviously, the amount of Nyquist-rate data is $N \times P$ and the amount of CS-MTMAB data is $M \times Q$. Thus the amount of data is reduced by $D_r \times D_a$ times compared to the traditional imaging algorithm.

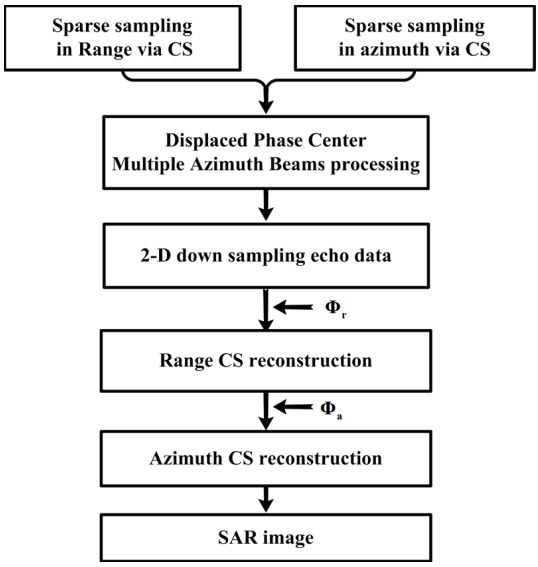

Figure 3. MTMAB SAR system with uniform displaced phase center sampling.

4. SIMULATION RESULTS

Simulated data have been used to validate the algorithm in this paper. Before the simulations, there are three key points to be aware of with this approach. First, the target space can be regarded as sparse in some special applications in which only a small number of strong scatters distribute in the illuminated scene, and the relatively few large coefficients of the scatterers can capture most of the information of scene, such as ocean ships monitoring, aircraft and spacecraft detecting, space debris imaging, and so on. The sparsity of the target scene is important in this proposed algorithm. Second, the measurement matrixes can be constructed by Equations (11) and (13). Third, we use the solution method of optimization directly as OMP [14]. In following experiments, we set the simulation radar parameters as listed in Table 1.

4.1. Point Scatterers Simulation

The simulated scene consists of five point targets. Point O is located in the center of the scene, and the other four targets are located on the vertices of a 500 m $\times$ 500 m square. The relative coordinates are listed as follows (m, m): $O\,(0, 0)$, $A\,(-100, -100)$, $B\,(100, -100)$, $C\,(-100, 100)$, $D\,(100, 100)$.

Using the parameters of Table 1, the 5 point targets are reconstructed via traditional MTMAB SAR imaging algorithm and CS-MTMAB algorithm, respectively. The results are shown in Figure 4. Figure 4(a) shows the SAR imaging results with traditional imaging algorithm based on Nyquist theory. The result of the

Table 1. Simulated radar parameters.

Parameters	Value
Antennas numbers	3
Carrier frequency	10 GHz
Transmitted signal bandwidth	150 MHz
Platform height	20 km
Platform velocity	1350 m/s
Pulse duration	10 μs
PRF	350 Hz
Range undersampling	4 times
Azimuth undersampling	4 times

proposed CS-MTMAB algorithm is shown in Figure 4(b). The results demonstrate that the proposed algorithm can give an exact recovery of the reflectivity function although the amount of data is reduced by 4×4 times, and also show that the presented CS-MTAMB method outperforms the conventional imaging algorithm based on matched filter method.

Furthermore, a point target located at the central scene is used for measurement. The results of the range and azimuth profile are shown in Figure 5. It illustrates that this method has better imaging performance in lower PSLR and ISLR than traditional reconstruction and also enhances the imaging quality.

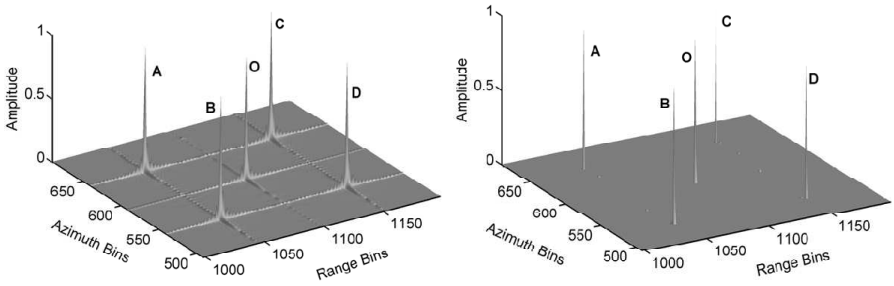

Figure 4. Comparison of imaging results obtained via two different methods. (a) 3-D reflectivity with traditional reconstruction. (b) 3-D reflectivity with the CS-MTMAB imaging algorithm.

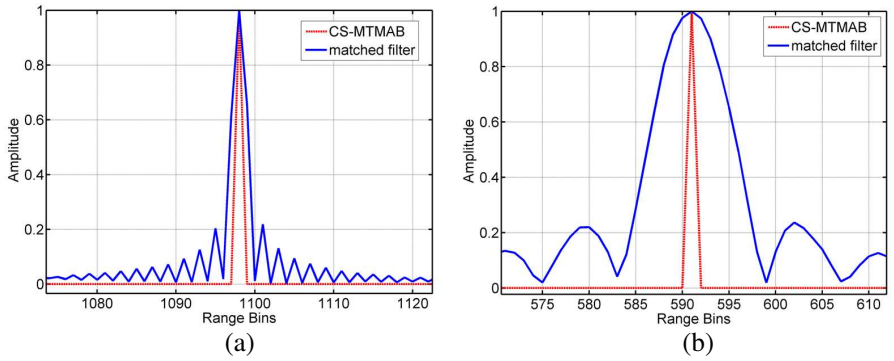

Figure 5. Range and azimuth compression simulation results. (a) Comparison of the range profile. (b) Comparison of the azimuth profile.

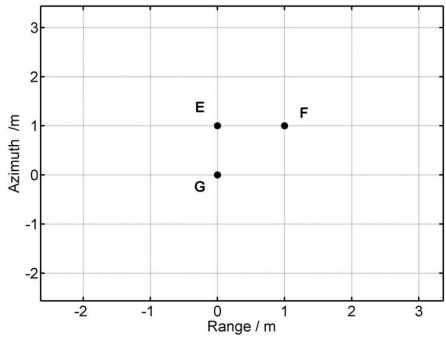

Figure 6. Simulated scene with three point targets.

4.2. Resolution Analysis

We show an important capability of this proposed method that is high resolution, which means that it can reconstruct image details under bandwidth limitations. To demonstrate this property, we apply our method on a synthetic scene composed of three point scatterers which are in different range and azimuth location. The coordinates of targets are listed as follows (m, m): $E\,(0, 1)$, $F\,(0, 0)$, $G\,(-1, 0)$ as shown in Figure 6.

This experiment uses the parameters of Table 1 and sets the traditional radar range resolution of 1.5 m, and azimuth resolution of 1.5 m. In this case, the traditional imaging algorithm can not distinguish the three point targets which their range and azimuth distance are 1 meter as Figure 7(a) shows. On the contrary, the proposed CS-MTMAB algorithm can clearly distinguish the targets as Figure 7(b) shows(after 8-times interpolation). In particular, the side-lobe image of Figure 7(b) is caused by the interpolation, and the original side-lobe image using CS-MTMAB is very small. This experiment illustrates CS theory would allow the implementation of wide-swath modes without reducing the resolution and have an enormous potential application in improving radar resolution.

4.3. Robustness and Noise Immunity

Using the parameters of Table 1 and setting 1 point target in simulated scene, the results in different signal to noise ratio (SNR) with traditional reconstruction and CS-MTMAB reconstruction are shown in Figure 8. Figures 8(a) and (c) show that the original targets are reconstructed when they separately probed with -10 dB and -20 dB additive white Gaussian noise (AWGN) via traditional

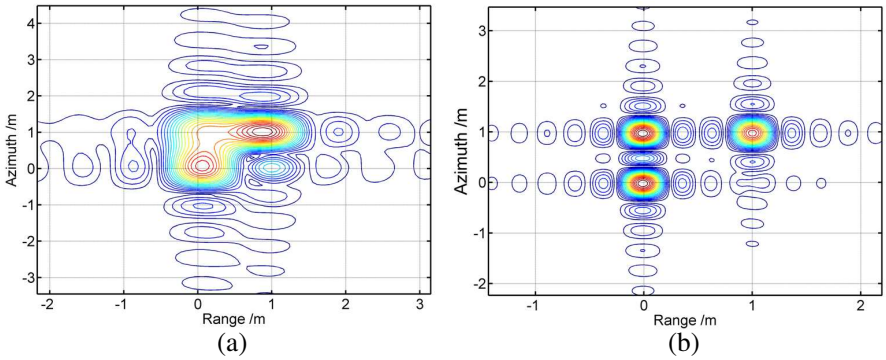

Figure 7. Comparison of contour plots using traditional and CSMTMAB algorithm. (a) Contour plots of targets E, F, and G using traditional algorithm after 8-times interpolation. (b) Contour plots of targets E, F and G using CS-MTMAB algorithm after 8-times interpolation.

imaging algorithm. Figures 8(b) and (d) illustrate their respective results in the presence of $-10\,\text{dB}$ and $-20\,\text{dB}$ of AWGN using CS-MTMAB algorithm. Compare the four figures, we can find out targets can be well reconstructed in presence of serious noise using CS-MTMAB algorithm. Therefore, the results clearly show that the performance of CS-MTMAB is high robustness and strong immunity in the presence of serious noise.

4.4. Performance Analysis

As mentioned above, D_r represents the range down-sampling times and D_a represents the azimuth down-sampling times. And the total down-sampling times β is defined as $D_r \cdot D_a$. The reconstruction error is calculated as $\|\hat{\mathbf{x}} - \mathbf{x}\|_2^2 / \|\mathbf{x}\|_2^2$, where $\hat{\mathbf{x}}$ and $\mathbf{x}$ are the estimated and true coefficient vectors, respectively. The experiment was repeated for different values of β and signal to noise ratio (SNR). The relationships between β, SNR and reconstruction error are depicted in Figure 9(a). As shown in Figure 9(a), it is clear that the CS-MTMAB algorithm can reconstruct targets in the case of serious down-sampling and low SNR level. Note that the error is extraordinary small for $\beta < 10$ and SNR $\geq -10\,\text{dB}$, and then increases rapidly for larger values of β and smaller values of SNR. Therefore, the proposed algorithm has high robustness in the presence of serious noise. Meanwhile, it is strongly immune to noise interference and has the characteristic of high noise immunity. These experimental results show that the proposed

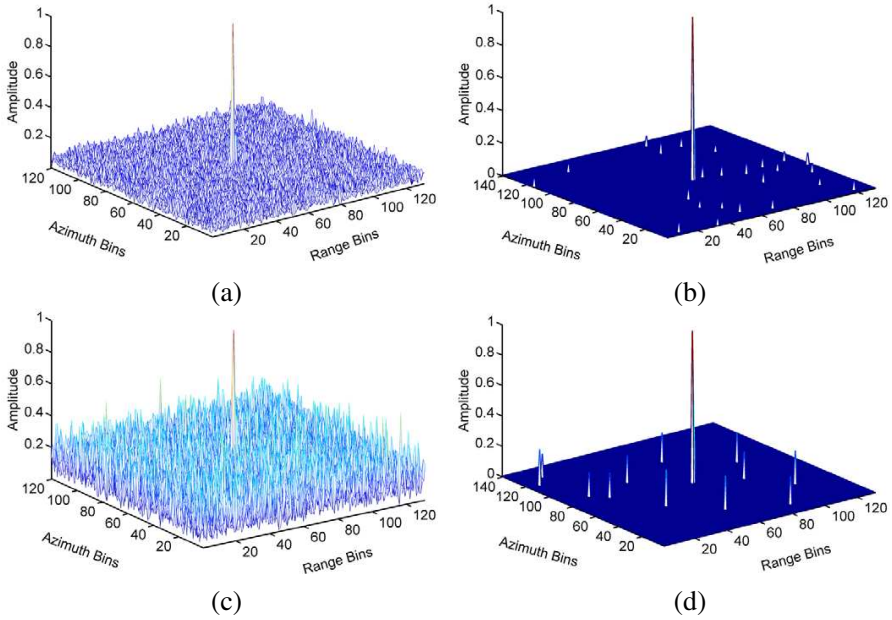

Figure 8. Comparison of reconstruction results with SNR. (a) Traditional reconstruction with −10 dB AWGN. (b) CS-MTMAB reconstruction with −10 dB AWGN. (c) Traditional reconstruction with −20 dB AWGN. (d) CS-MTMAB reconstruction with −20 dB AWGN.

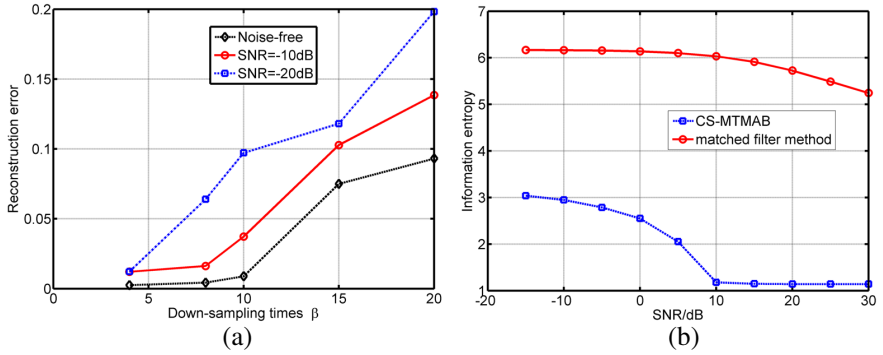

Figure 9. The results of performance analysis. (a) Reconstruction error for different β and SNR. (b) Relation between information entropy and SNR.

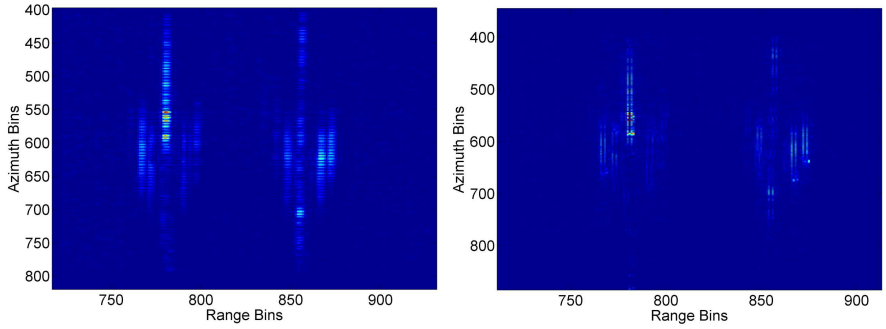

Figure 10. The results of real raw data with CS-MTMAB and conventional algorithm. (a) The conventional algorithm with full sampled data. (b) CS-MTMAB with 25% sampled data.

algorithm is valid under certain conditions.

The following will be given a new evaluation method based on information entropy. The information entropy can be calculated as $\Gamma = -\sum_{i=1}^{P}\sum_{j=1}^{N} p_{ij}\log p_{ij}$, where $p_{ij} = |A(i,j)| \,/\, \sum_{i=1}^{P}\sum_{j=1}^{N} |A(i,j)|$ and $A(i, j)$ represents the amplitude of the reconstructed results based on CS. The information entropy is the measured standard of the information. The smaller value of the information entropy we get, the higher experiment measurement quality of the results will be. The relationship between information entropy and different SNR level is shown in Figure 9(b). From Figure 9(b), we can see that the noise in the echo may be restrained with increasing of SNR. It is because the information redundancy of the measured echo signals is declining with the increasing of the SNR, so the reconstructed performance would be better. Moreover, we can also get the conclusion that the proposed CS-MTMAB SAR imaging results are far better than the traditional MTMAB SAR imaging results.

4.5. Imaging with Real Raw Data

Some experimental results as shown in Figure 10, obtained by processing real raw airborne SAR data with CS-MTMAB and conventional approach are presented. The real raw data scene is an airport with two aircrafts which can be seen as strong scattering targets in the scene. Thus the target scene is sparse and we can apply the propose method to the real raw data. The transmitted

signal bandwidth is 200 MHz, the pulse duration is 30 μs, the platform velocity is 105 m/s, and the PRF is 1000 Hz.

Figure 10(a) shows the result with traditional imaging algorithm. The result with 25% sampled data using CS-MTMAB are shown in Figure 10(b). Compared with the Figure 10, we can find that the proposed algorithm can accurately focus the aircrafts in the sparse scene although the sampled data is reduced by 4 times. This real raw data experiment illuminates that this proposed method is of great significance to the sparse targets imaging such as sea ship targets imaging, aircraft and spacecraft detecting and space debris imaging. It can storage space and transmission bandwidth in many application fields, particularly in systems having real-time imaging capability.

5. CONCLUSION

In this paper, a novel 2-D SAR imaging algorithm is proposed based on constructing measurement matrixes in range and azimuth dimensions via compressed sensing techniques, respectively. And the MTMAB technology is used in this algorithm to resolve the contradiction between high resolution and wide-swath. This radar system randomly transmits fewer pulses in azimuth and samples fewer data than traditional systems at random intervals in range. Thereby, this method provides a new approach of receiving echo data via 2-D random sparse sampling with a significant reduction in the number of sampled data beyond the Nyquist theorem. This will directly impact A/D conversion, and has the potential to reduce the overall data rate and to simplify hardware design. The simulation results, real raw airborne SAR data experiment and performance analysis verify the validity of the proposed CS-MTMAB imaging algorithm which is lower PSLR and ISLR, less sampled data, higher resolution, stronger robustness and higher noise immunity than the traditional SAR imaging algorithm.

ACKNOWLEDGMENT

This work was supported by the Fundamental Research Funds for the Central Universities of China under NO. ZYGX2010J118.

REFERENCES

1. Chan, Y. K. and V. C. Koo, "An introduction to synthetic aperture radar (SAR)," *Progress In Electromagnetics Research B*, Vol. 2, 27–60, 2008.

2. Currie, A. and M. A. Brown, "Wide swath SAR," *Proc. Inst. Electr. Eng. F — Radar Signal Process.*, Vol. 139, No. 2, 122–135, 1992.
3. Currie, A., "Wide-swath SAR imaging with multiple azimuth beams," *IEE Colloquium on Synthetic Aperture Radar*, Vol. 29, 3/1–3/4, London, 1989.
4. Delaurentis, J., "Multipath synthetic aperture radar imaging," *IEE Radar, Sonar and Navig.*, Vol. 5, No. 5, 561–572, 2011.
5. Wu, W., P. Huang, and Y.-K. Deng, "Multi-channel specmb-tops SAR for high-resolution wide-swath imaging," *Progress In Electromagnetics Research*, Vol. 116, 533–551, 2011.
6. Lim, S.-H., J.-H. Han, S.-Y. Kim, and N.-H. Myung, "Azimuth beam pattern synthesis for airborne SAR system optimization," *Progress In Electromagnetics Research*, Vol. 106, 295–309, 2010.
7. Xu, W., P. Huang, and Y.-K. Deng, "MIMO-tops mode for high-resolution ultra-wide-swath full polarimetric imaging," *Progress In Electromagnetics Research*, Vol. 121, 19–37, 2011.
8. Donoho, D. L., "Compressed sensing," *IEEE Trans. on Information Theory*, Vol. 52, No. 4, 1289–1306, Apr. 2006.
9. Candès, E. J. and M. Wakin, "An introduction to compressive sampling," *IEEE Signal Processing Magazine*, Vol. 52, No. 4, 21–30, Mar. 2008.
10. Candès, E. J., J. Romberg, and T. Tao, "Robust uncertainty principles: Exact signal reconstruction from highly incomplete frequency information," *IEEE Trans. on Information Theory*, Vol. 52, No. 2, 489–509, Feb. 2006.
11. Romberg, J., "Imaging via compressive sampling," *IEEE Signal Processing Magazine*, 14–20, Mar. 2008.
12. Baraniuk, R. and P. Steeghs, "Compressive radar imaging," *IEEE Radar Conf.*, 128–133, Waltham, MA, Apr. 2007.
13. Herman, M. and T. Strohmer, "High resolution radar via compressed sensing," *IEEE Trans. on Signal Process.*, Vol. 57, No. 6, 2275–2284, Jun. 2009.
14. Varshney, K., M. Cetin, J. Fisher, and A. Willsky, "Sparse representation in structured dictionaries with application to synthetic aperture radar," *IEEE Trans. on Signal Process.*, Vol. 56, No. 8, 3548–4561, Aug. 2008.
15. Patel, V., G. Easley, D. Healy, and R. Chellappa, "Compressed synthetic aperture radar," *IEEE Journal of Selected Topics in Signal Processing*, Vol. 4, No. 2, 244–254, Apr. 2010.

16. Wei, S.-J., X.-L. Zhang, J. Shi, and G. Xiang, "Sparse reconstruction for SAR imaging based on compressed sensing," *Progress In Electromagnetics Research*, Vol. 109, 63–81, 2010.
17. Wei, S.-J., X.-L. Zhang, and J. Shi, "Linear array SAR imaging via compressed sensing," *Progress In Electromagnetics Research*, Vol. 117, 299–319, 2011.
18. Ender, J., "On copressed sensing applied to radar," *Elsevier Signal Process.*, Vol. 90, No. 5, 1402–1414, May 2010.
19. Candès, E. J., "The restricted isometry property and its implications for compressed sensing," *C. R. Acad. Sci. Paris*, Ser. I, 589–592, 2008.
20. Kreger, G., N. Gebert, and A. Moreira, "Unambiguous SAR signal reconstruction from nonuniform displaced phase center sampling," *IEEE Geoscience and Remote Sensing Letters*, Vol. 1, No. 4, 260–264, Oct. 2004.